SECRET

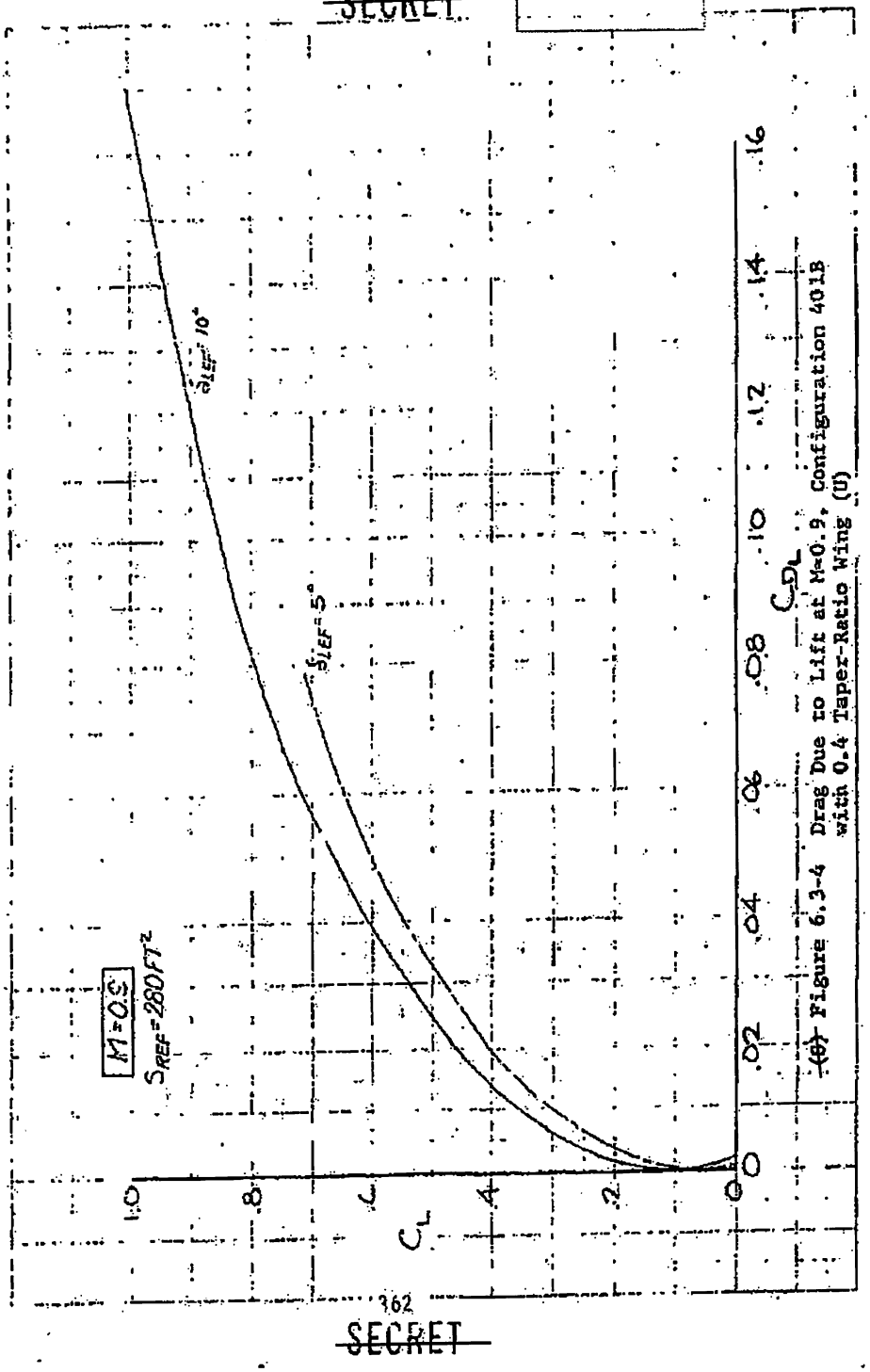

(U) Figure 6.3-4 Drag Due to Lift at M=0.9, Configuration 401B with 0.4 Taper-Ratio Wing

SECRET

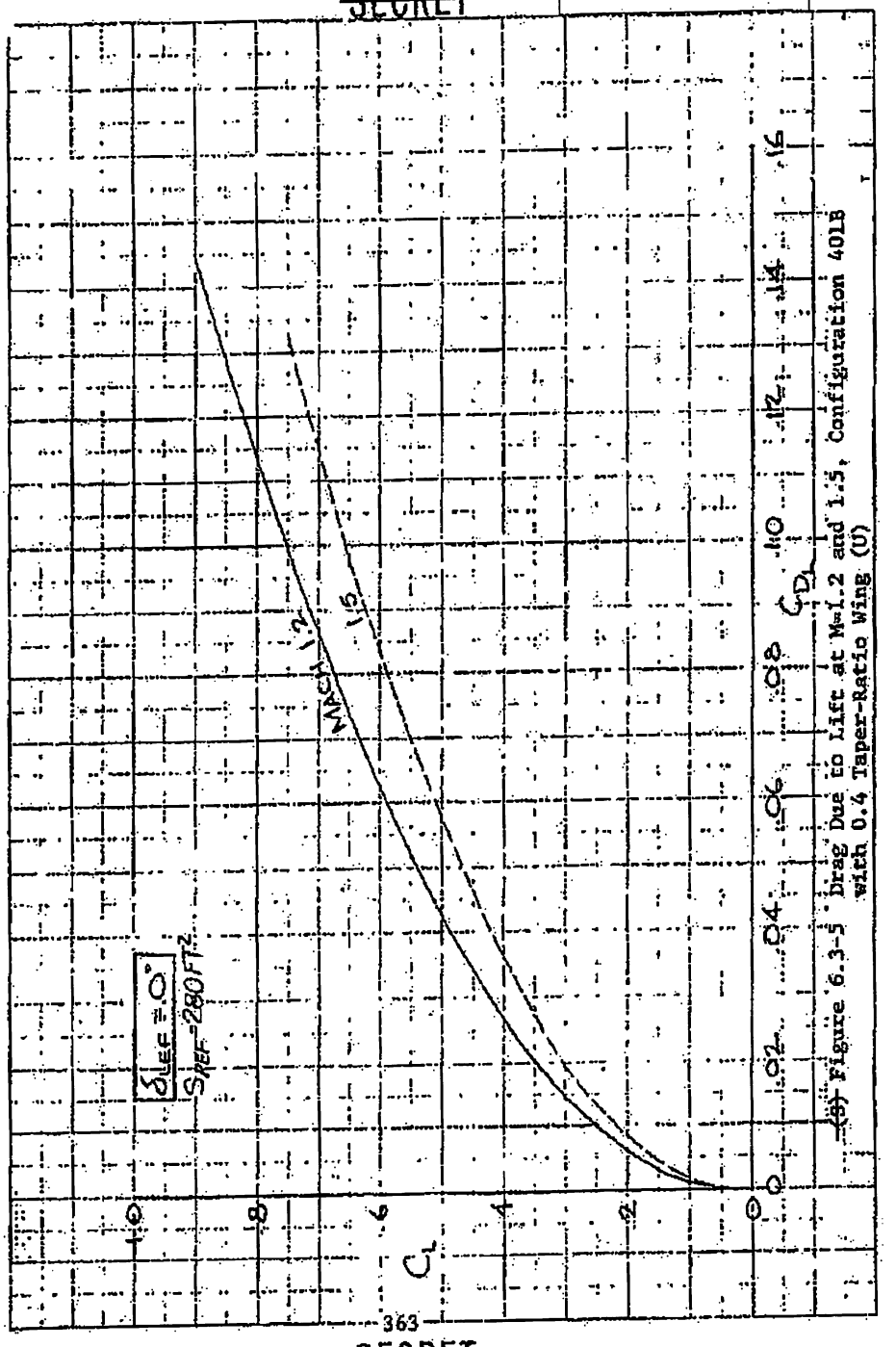

(U) Figure 6.3-5 Drag Due to Lift at M=1.2 and 1.5, Configuration 401B with 0.4 Taper-Ratio Wing (U)

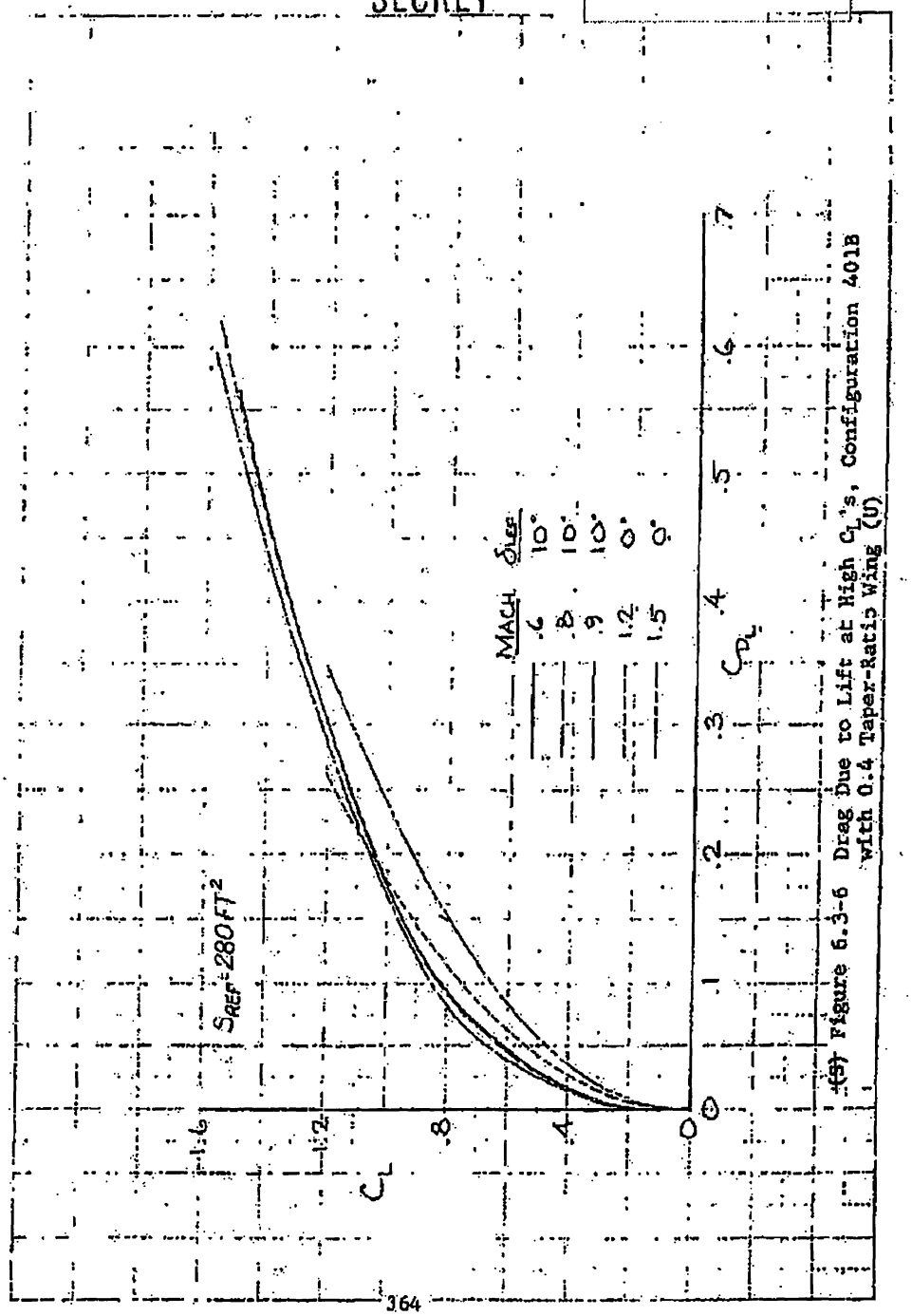

(S) Figure 6.3-6 Drag Due to Lift at High C_L's, Configuration 401B with 0.4 Taper-Ratio Wing (U)

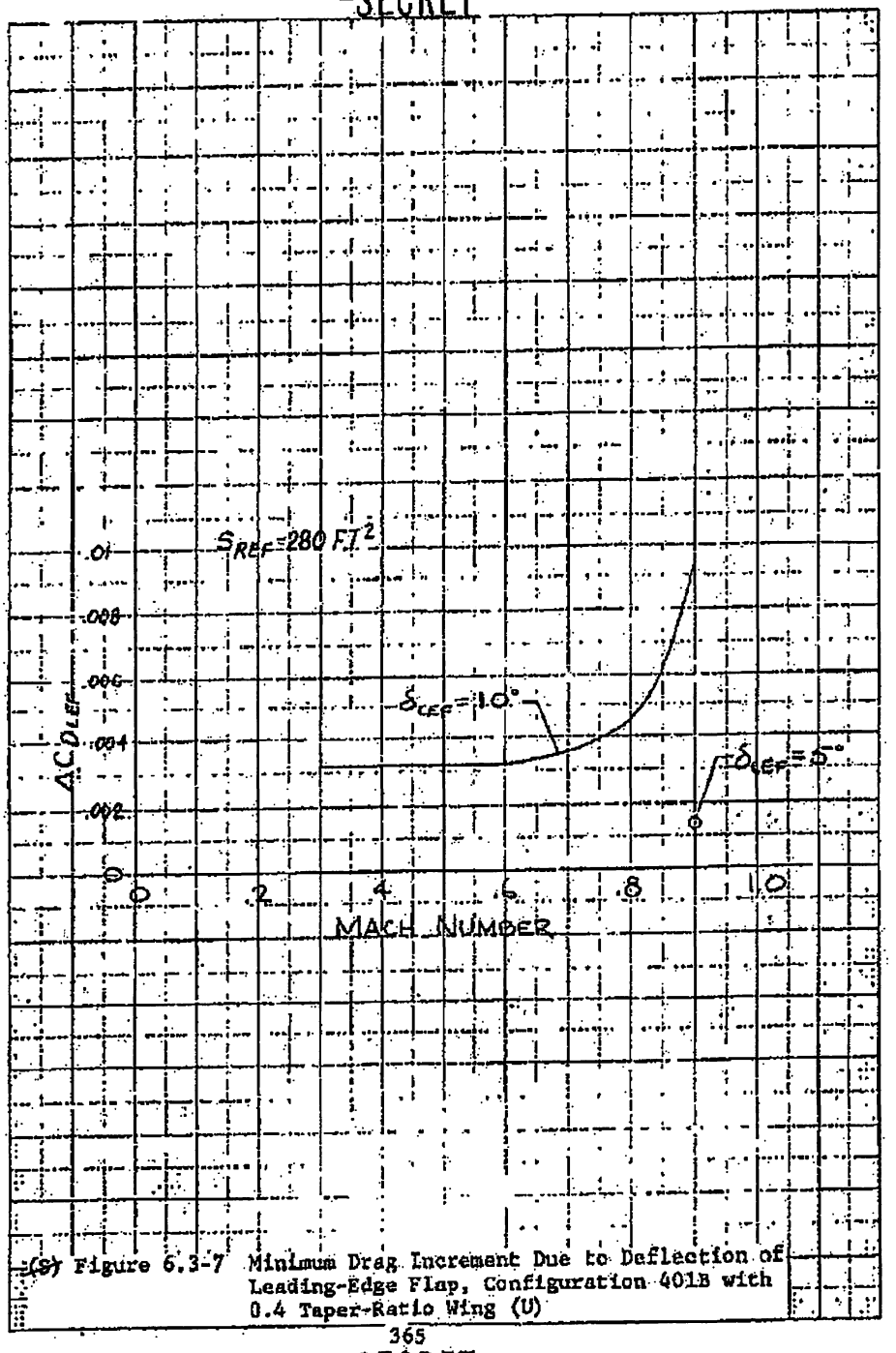

(S) Figure 6.3-7 Minimum Drag Increment Due to Deflection of Leading-Edge Flap, Configuration 401B with 0.4 Taper-Ratio Wing (U)

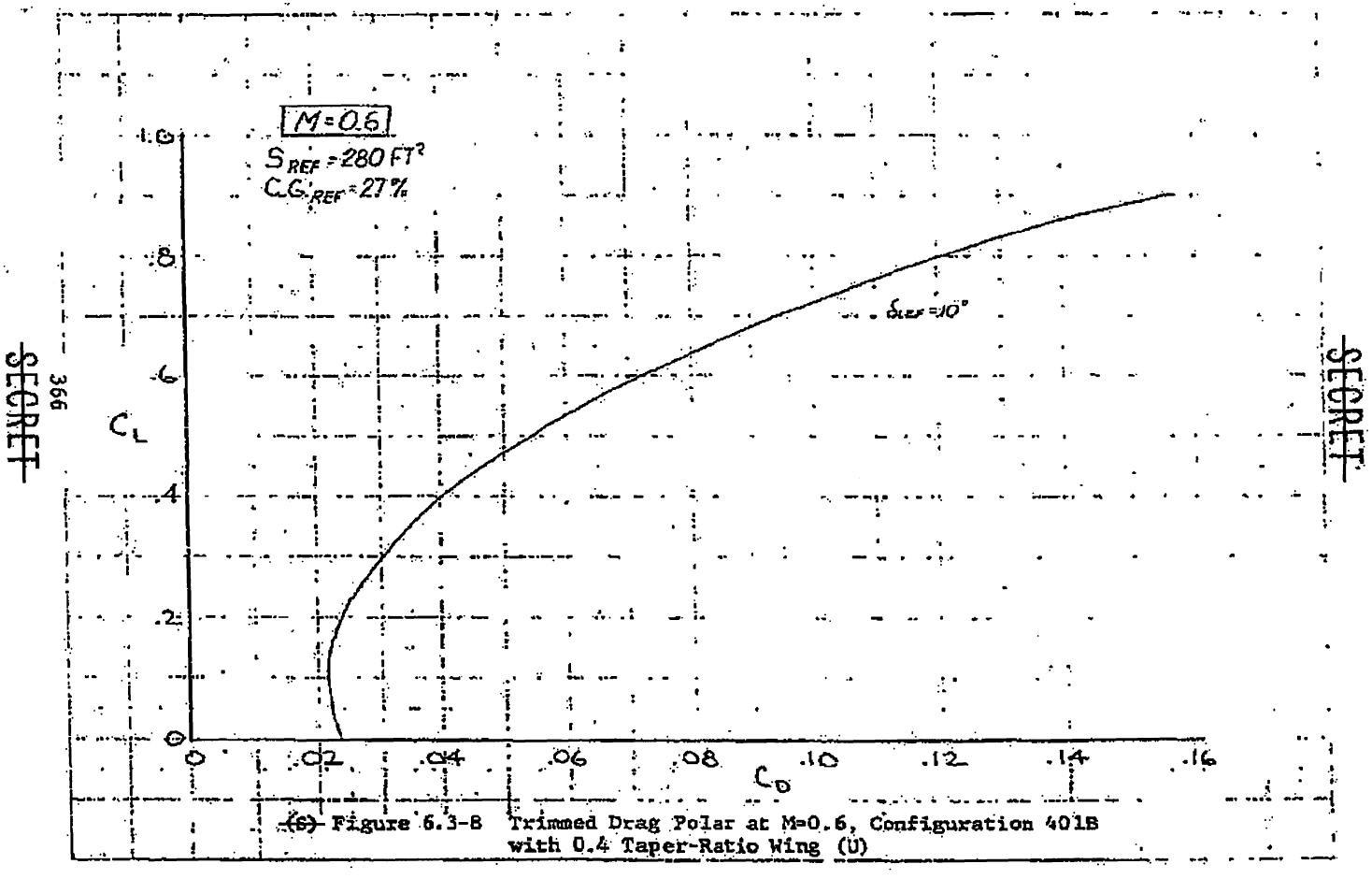

(S) Figure 6.3-8 Trimmed Drag Polar at M=0.6, Configuration 401B with 0.4 Taper-Ratio Wing (U)

SECRET

366

SECRET

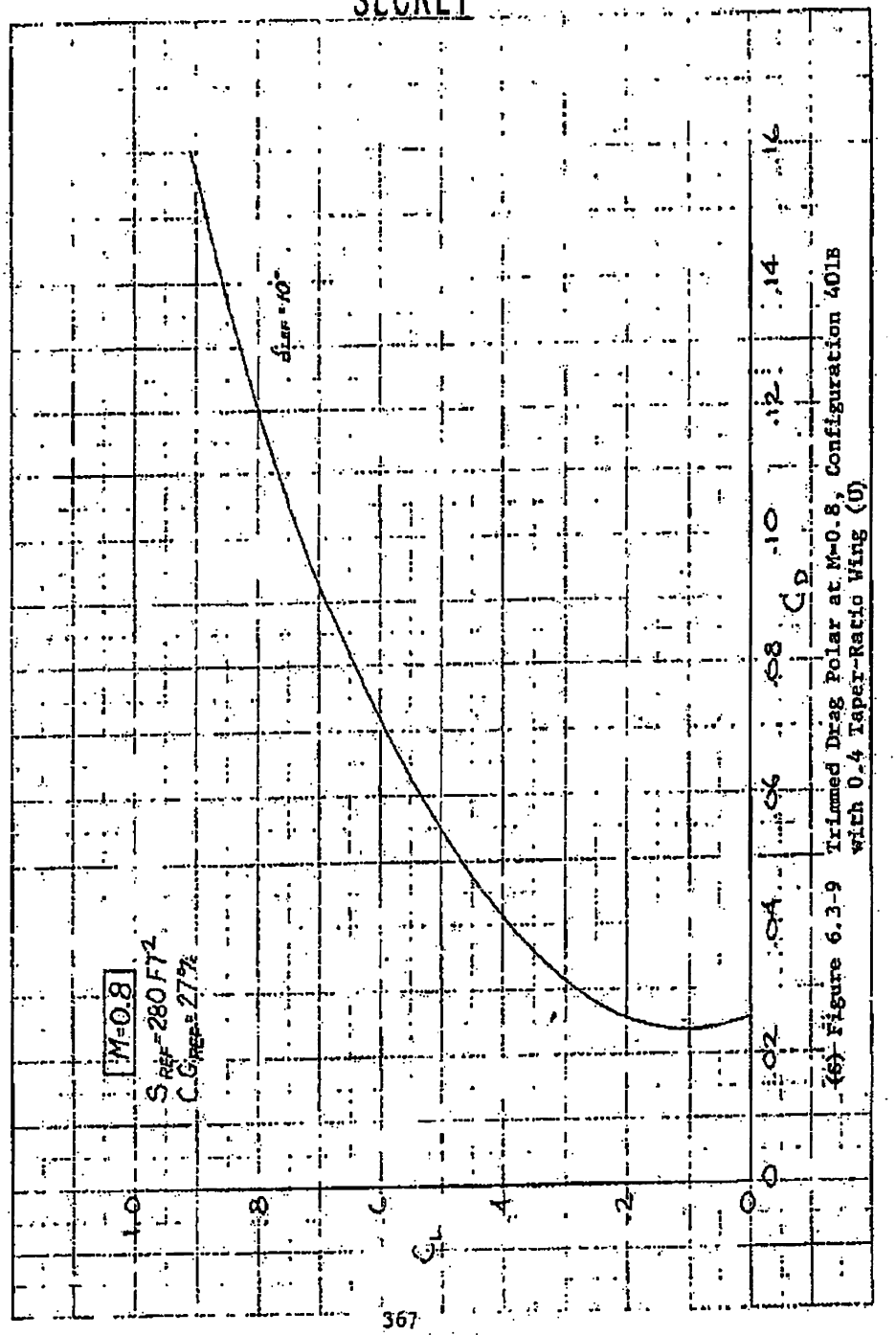

(U) Figure 6.3-9 Trimmed Drag Polar at M=0.8, Configuration 401B with 0.4 Taper-Ratio Wing (U)

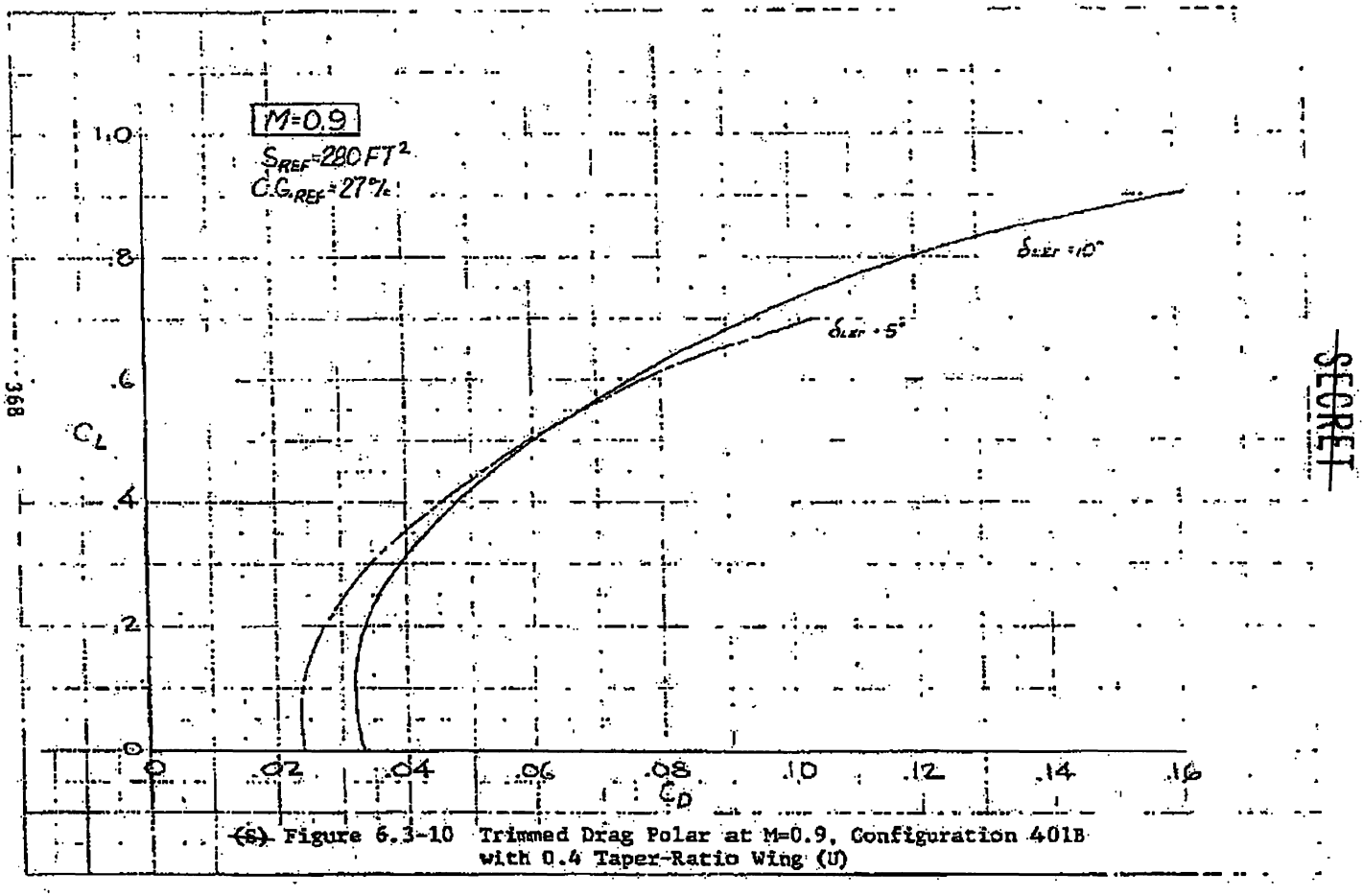

(S) Figure 6.3-10 Trimmed Drag Polar at M=0.9, Configuration 401B with 0.4 Taper-Ratio Wing (U)

(S) Figure 6.3-11 Trimmed Drag Polar at M=1.2 and 1.5, Configuration 401B with 0.4 Taper-Ratio Wing (U)

SECRET

SECRET

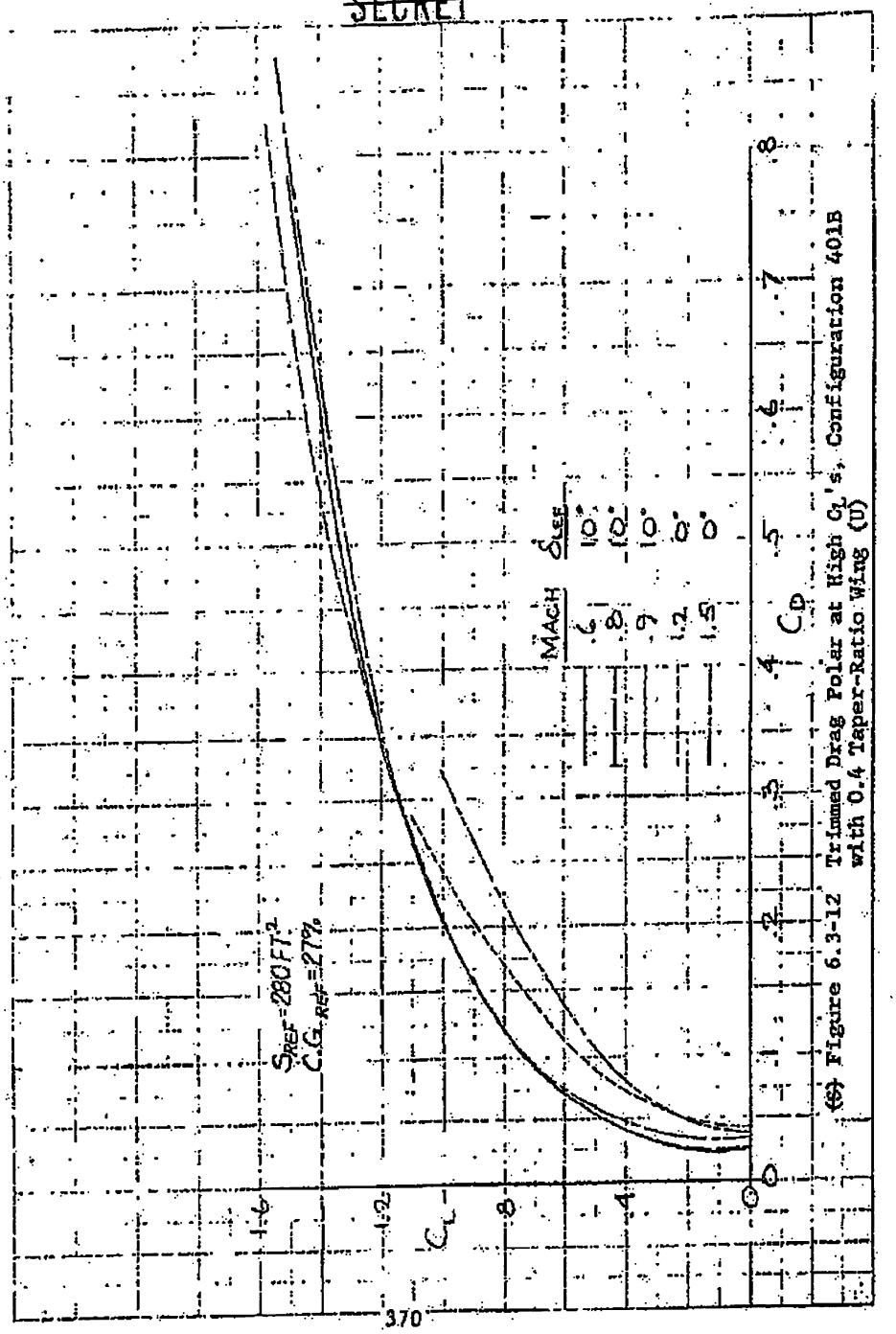

(U) Figure 6.3-12 Trimmed Drag Polar at High C_L's, Configuration 401B with 0.4 Taper-Ratio Wing (U)

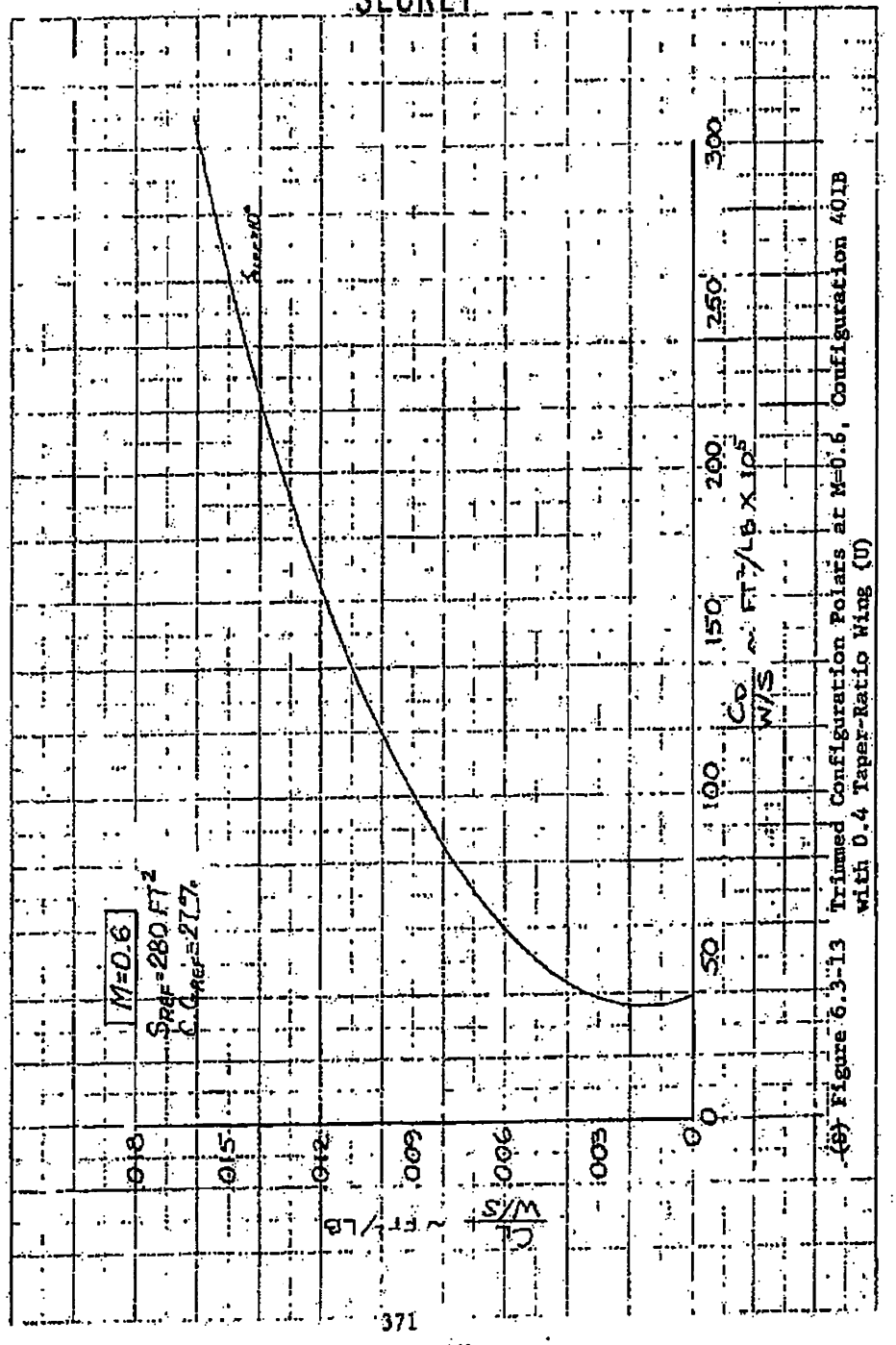

(U) Figure 6.3-13 Trimmed Configuration Polars at M=0.6, Configuration 401B with 0.4 Taper-Ratio Wing (U)

(S) Figure 6.3-14 Trimmed Configuration Polars at M=0.8, Configuration 401B with Taper-Ratio Wing (U)

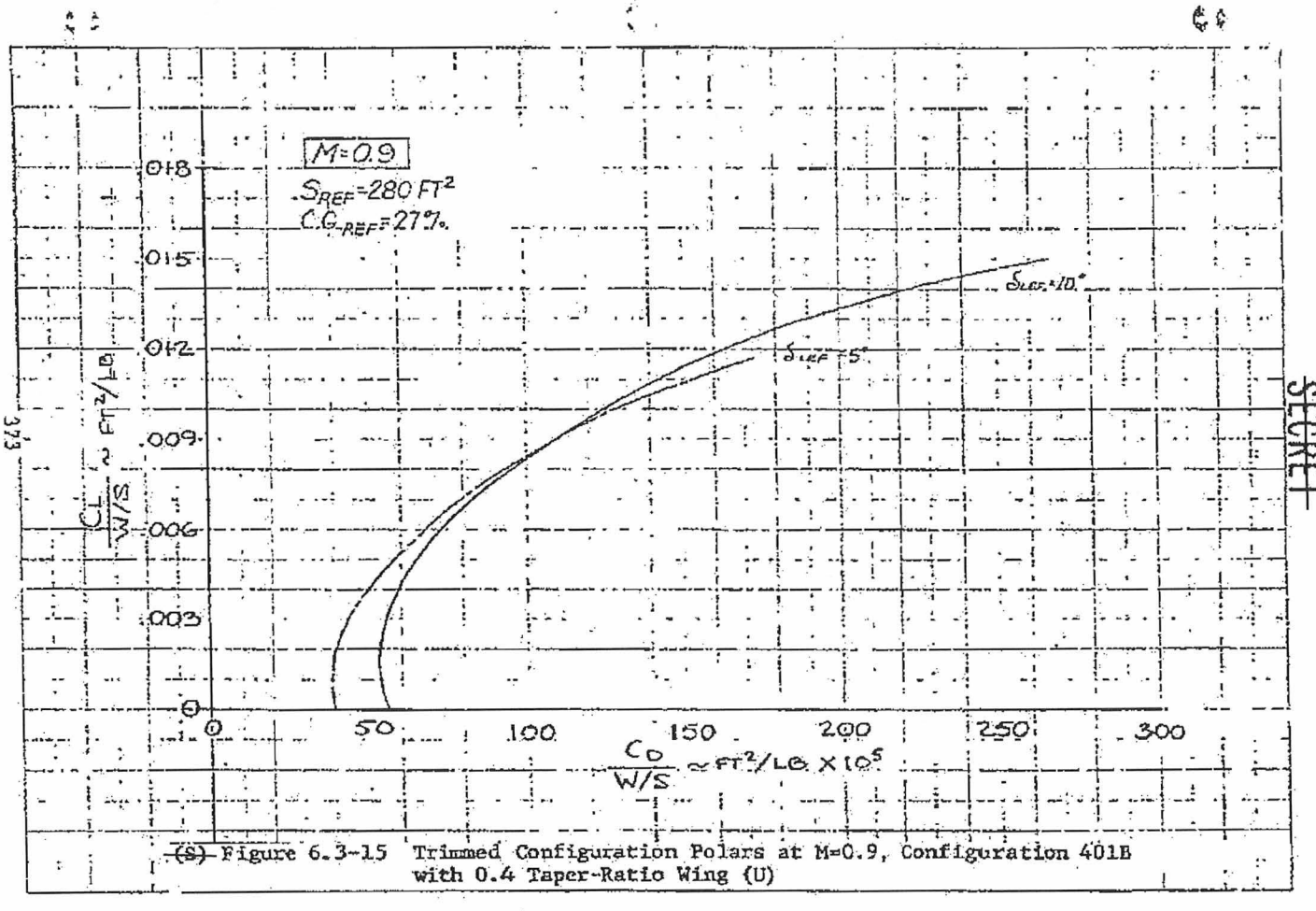

(S) Figure 6.3-15 Trimmed Configuration Polars at M=0.9, Configuration 401B with 0.4 Taper-Ratio Wing (U)

SECRET

373

SECRET

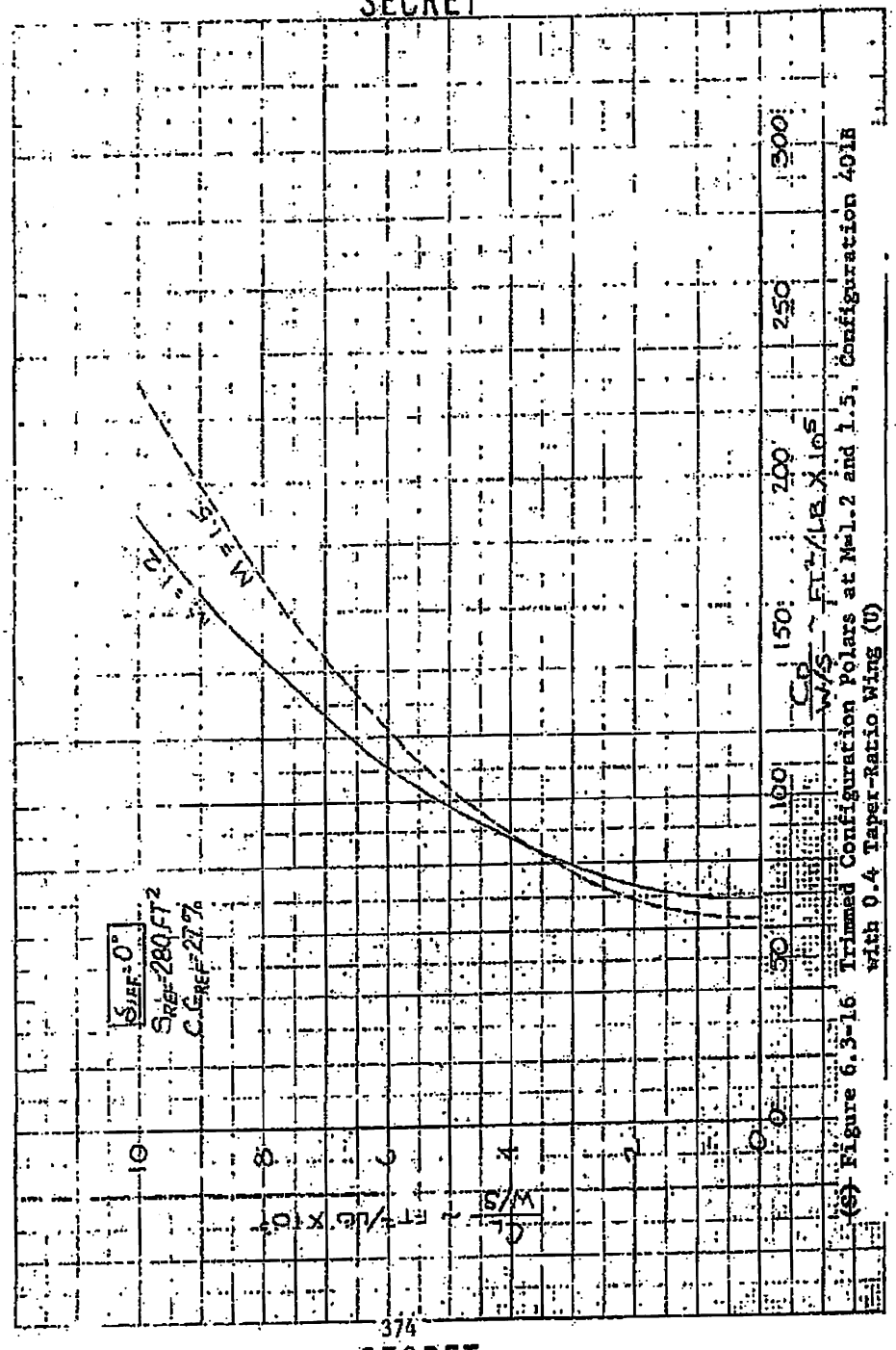

(S) Figure 6.3-16. Trimmed Configuration Polars at M=1.2 and 1.5, Configuration 401B with 0.4 Taper-Ratio Wing (U)

(S) Figure 6.3-17 Trimmed Configuration Polars at High C_L's, Configuration 401B with Taper-Ratio Wing (U)

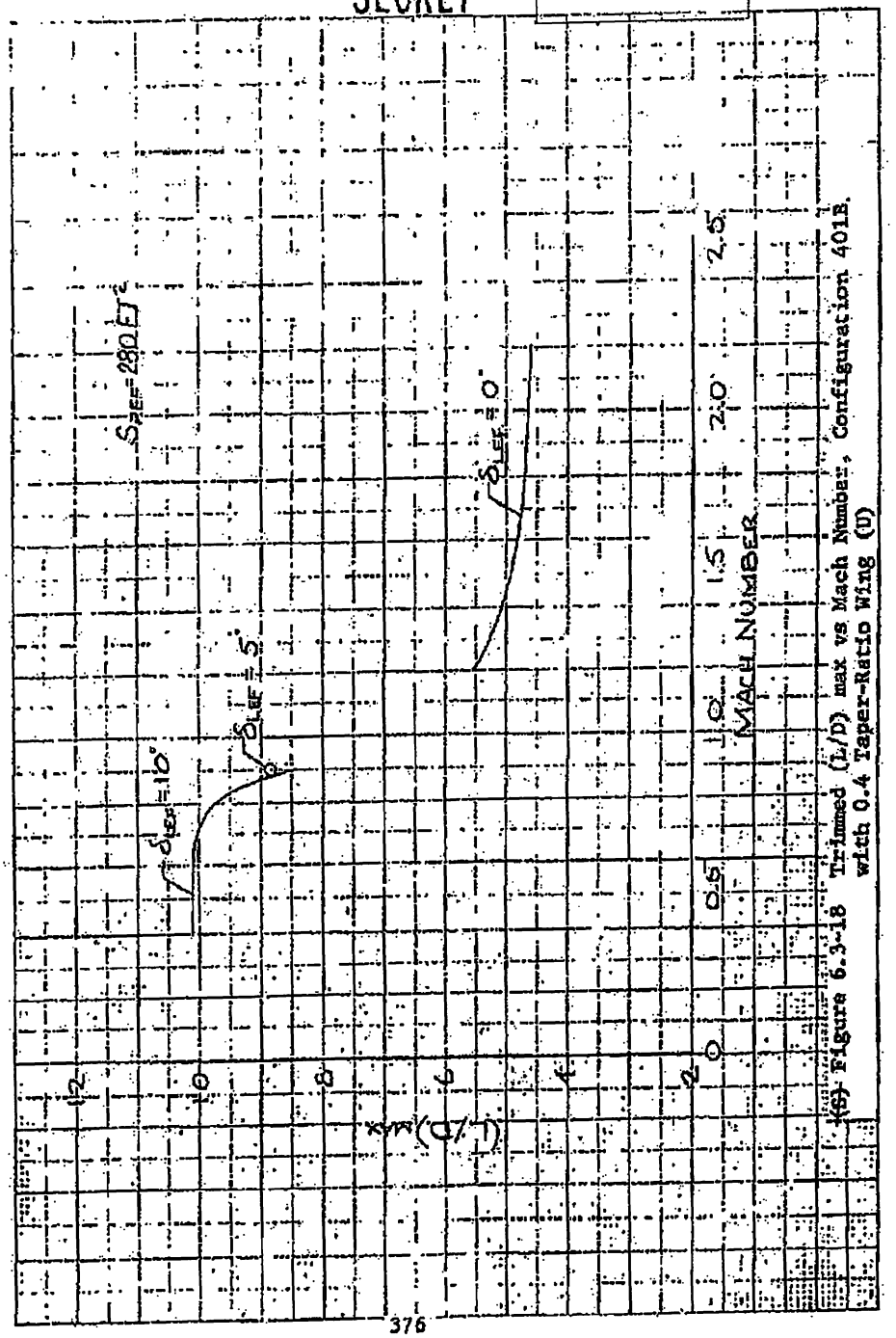

(U) Figure 6.3-18 Trimmed (L/D) max vs Mach Number, Configuration 401E with 0.4 Taper-Ratio Wing (U)

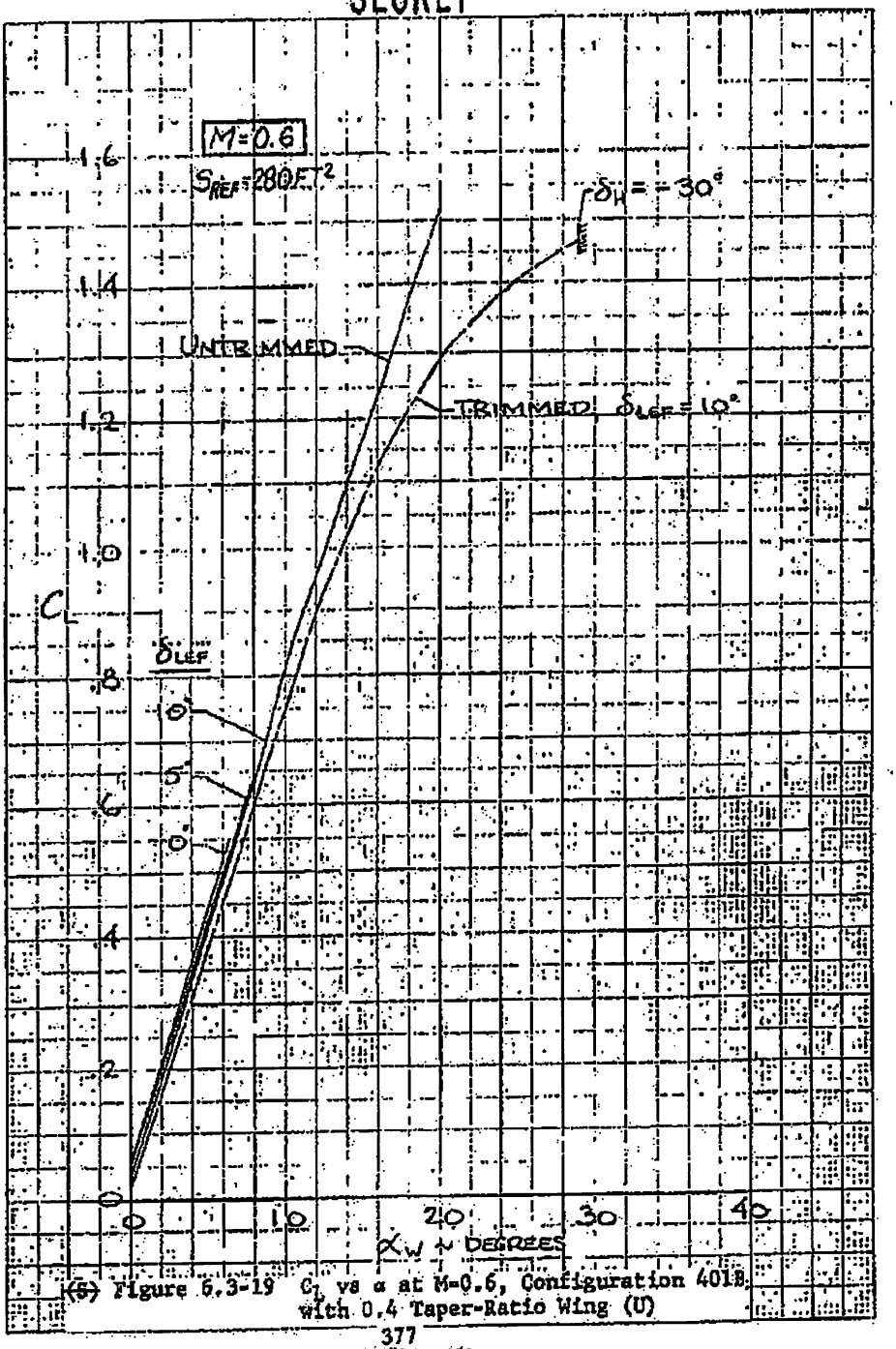

(S) Figure 6.3-19 C_L vs α at M=0.6, Configuration 4018 with 0.4 Taper-Ratio Wing (U)

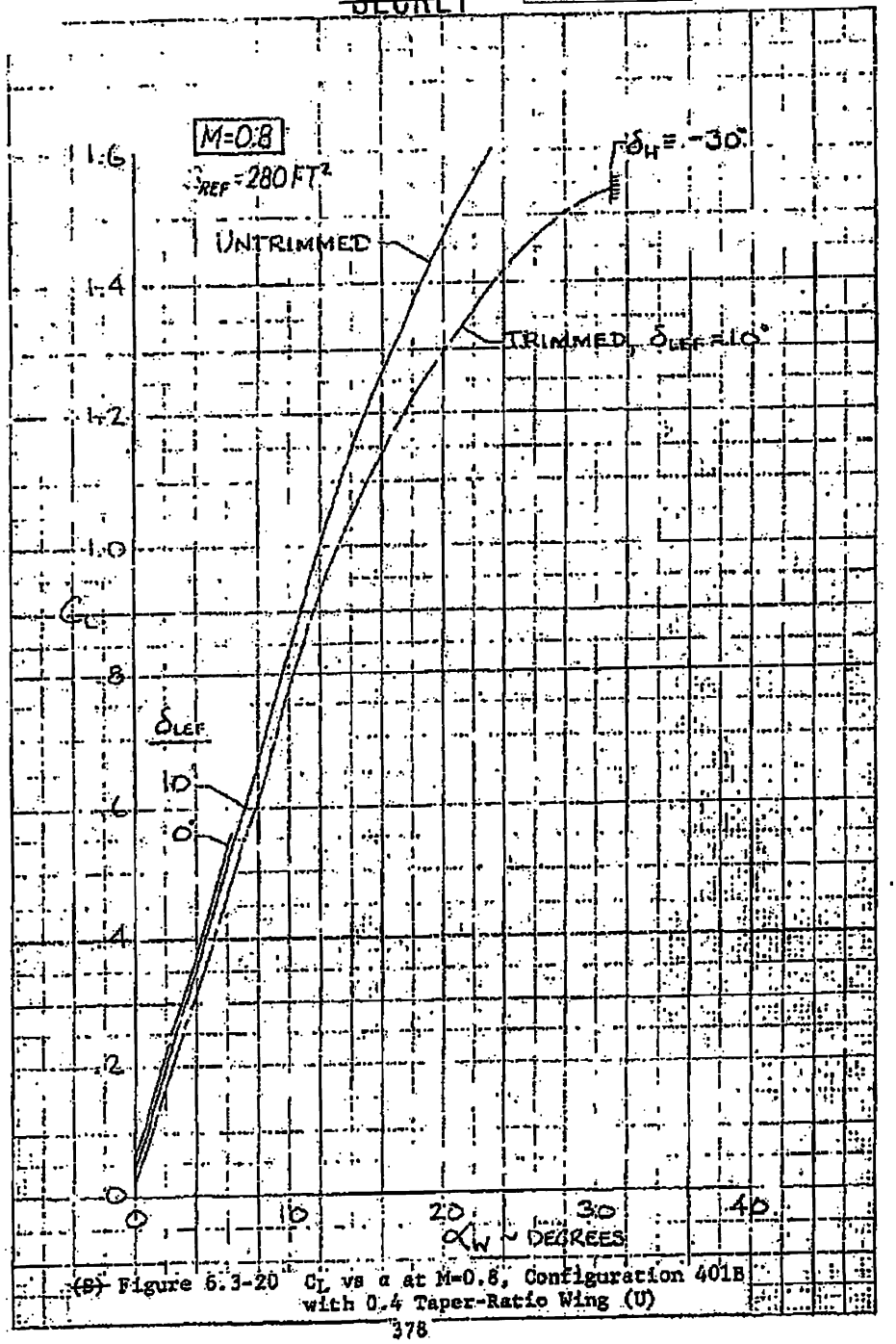

~~(S)~~ Figure 6.3-20 C_L vs α at M=0.8, Configuration 401B with 0.4 Taper-Ratio Wing (U)

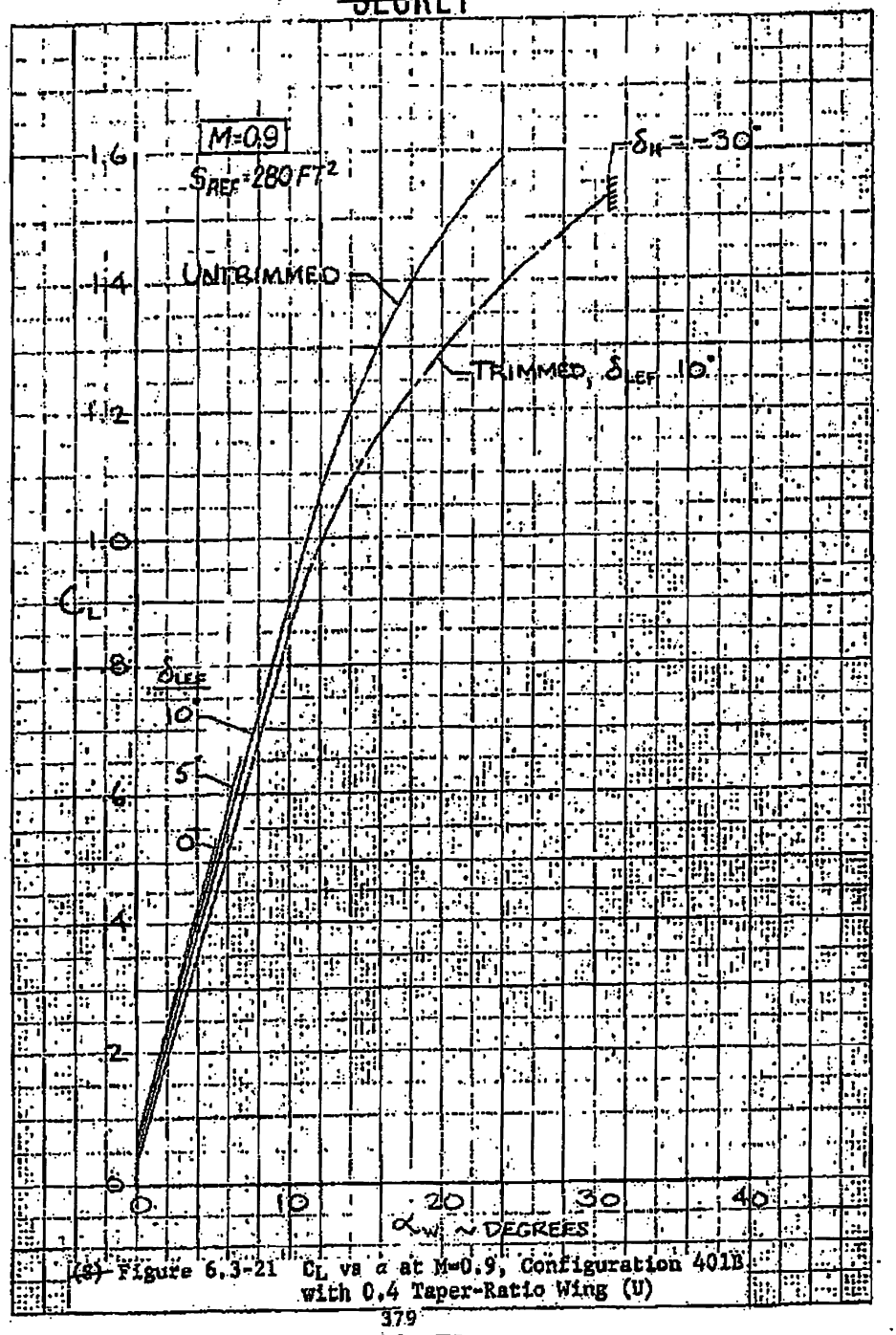

(S) Figure 6.3-21 C_L vs α at M=0.9, Configuration 401B with 0.4 Taper-Ratio Wing (U)

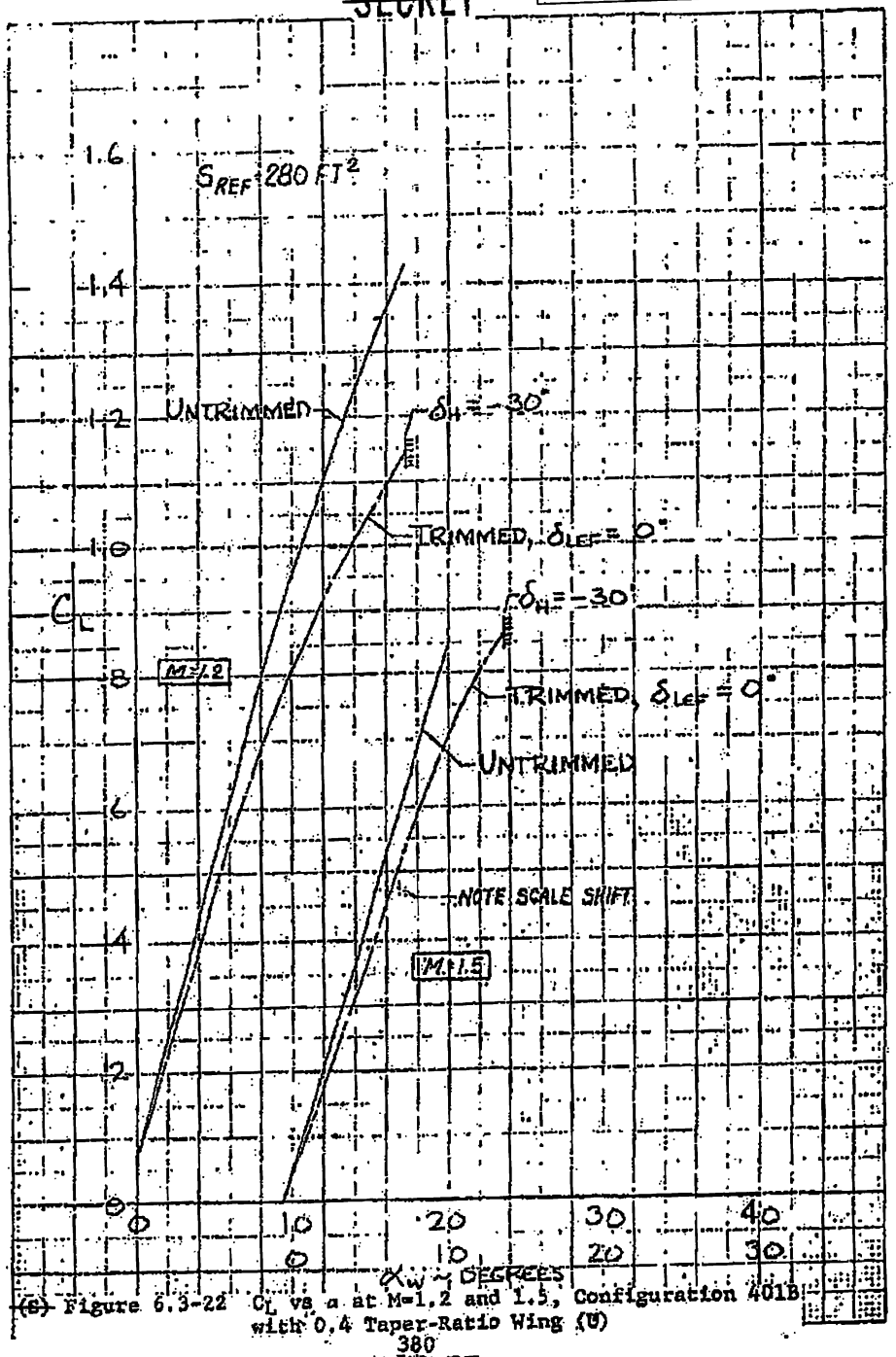

(S) Figure 6.3-22 C_L vs α at M=1.2 and 1.5, Configuration 401B with 0.4 Taper-Ratio Wing (U)

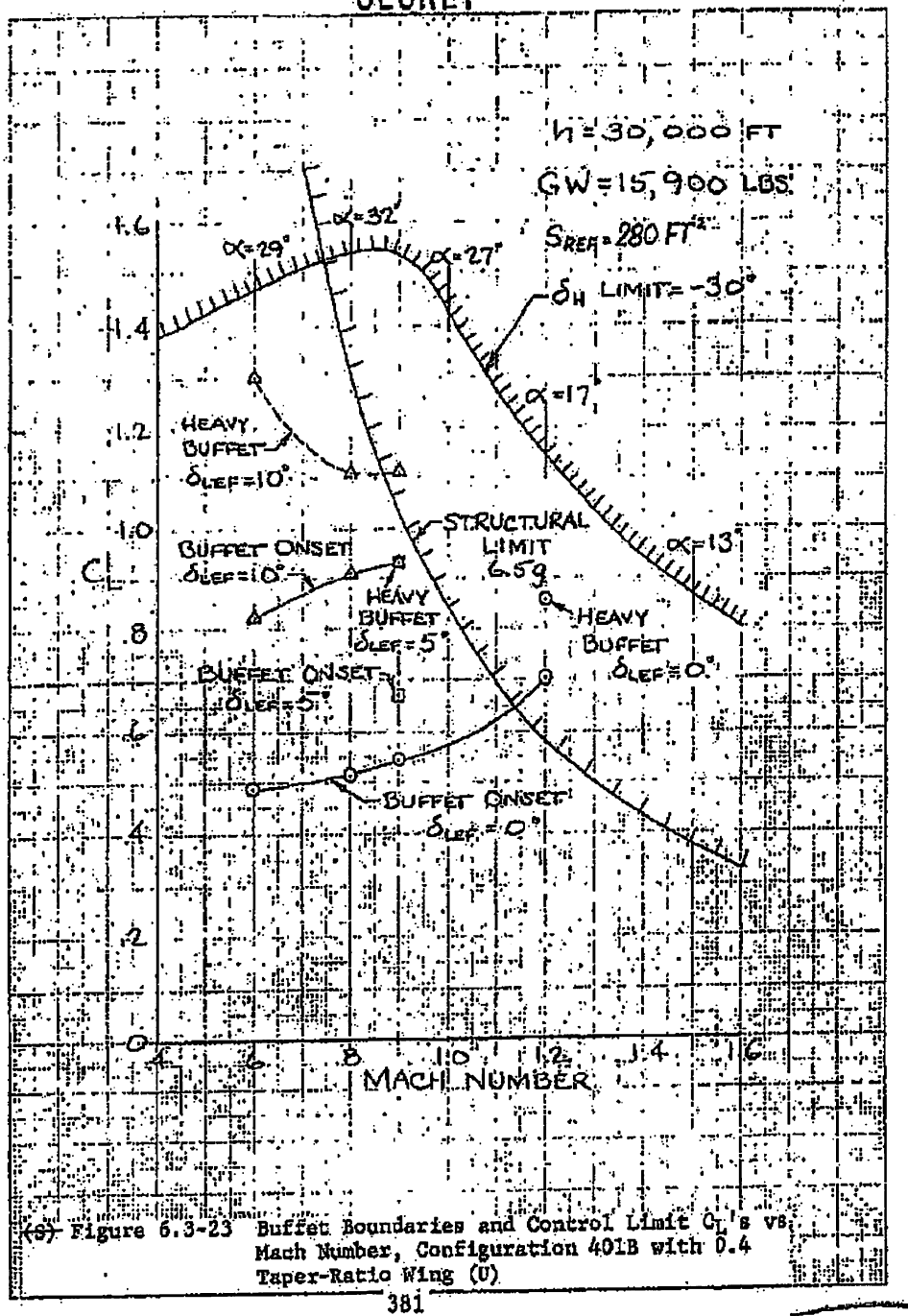

(S) Figure 6.3-23 Buffet Boundaries and Control Limit C_L's vs Mach Number, Configuration 401B with 0.4 Taper-Ratio Wing (U)

6.4 STABILITY, CONTROL, AND HANDLING QUALITIES

(U) The basic stability and handling qualities of Configuration 401B were not significantly altered by the change in wing taper ratio from 0.2 to 0.4. Since the leading-edge sweep angle and aspect ratio were held constant, the increased taper ratio shifted the wing area aft. The net change in longitudinal stability was very small, however, because the trailing-edge sweep angle changed with taper ratio and the consequent change in cutout factor was compensatory. Similarly, since the configuration was essentially identical in other respects, there are no changes in lateral-directional stability attributable to the increased taper ratio. As a result, the stability and control characteristics and handling qualities reported in Section 3.4 for the basic 401B configuration are also directly applicable to the 0.4 taper-ratio fighter.

6.5 STRUCTURES AND WEIGHTS

~~(S)~~ Weight analysis for the 0.4 taper-ratio wing on Configuration 401B was performed in the same manner as the weight analyses described in previous sections (see Section 3.5). The 16,800-pound configuration was used to evaluate this wing with a structural design gross weight (80% fuel) of 15,960 pounds and a ferry mission overload gross weight of 27,000 pounds.

~~(S)~~ Input data for the weight equations were derived from the data presented in Section 6.1. The statement of work specifies a 4% thickness-to-chord ratio for this wing. In order to achieve a minimum weight, this 4% thickness was interpreted to be an RMS thickness of 4%, which results in a thickness-to-chord ratio of 2.5% at the tip and 4.84% at Buttock Line 54, the start of the expanded root section. This interpretation resulted in a wing structural weight decrement of 151 pounds.

~~(S)~~ A weight summary for this configuration is shown in Table 6.5-1. A summary of the center-of-gravity conditions for the various missions is shown below.

Condition	Basic Operating Weight	Zero Fuel Weight	Gross Weight
SRASM			
Weight (lb)	12,226	12,859	16,800
C.G. (% MAC)	23.9	23.1	20.0
LRASM			
Weight (lb)	13,074	13,707	21,638
C.G. (% MAC)	24.0	23.3	21.2
Ferry Mission			
Weight (lb)	13,916	14,201	27,000
C.G. (% MAC)	23.9	22.7	21.7

~~(S)~~ Table 6.5-1 WEIGHT SUMMARY: CONFIGURATION 401B WITH 0.4 TAPER RATIO WING (pounds) (U)

Item	Weight
Structure	(5529)
Wing	1687
Fuselage	2588
Horizontal Tail	322
Vertical Tail	316
Landing Gear	616
Propulsion	(3530)
Engine	2737
Air Induction	322
Fuel System	421
Engine Controls	22
Starting System	28
Systems and Equipment	(2767)
Surface Controls	612
Landing Gear Controls	115
Instruments	94
Hydraulics and Pneumatics	283
Electrical	370
Avionics	460
Furnishings	238
Air Conditioning System	142
Armament	453
Weight Empty	11,826
Useful Load	(400)
Crew	200
Unuseable fuel	23
Engine Oil	17
Missile Racks and Pylons	124
Miscellaneous	36
Basic Operating Weight	12,226
Payload	(633)
Ammo (500 Rounds)	285
Missiles (2)	348
Zero Fuel Weight	12,859
Fuel	3941
Gross Weight	16,800

SECTION 7

SUPERCRITICAL WING STUDY

(U) The supercritical wing, which is an outgrowth of recent advances in transonic aerodynamic technology, has been evaluated on Configuration 401B to determine its potential for improved transonic maneuverability. The supercritical wing study was conducted in two phases:

1. An abbreviated wing-planform parametric study was conducted to select the planforms having the most potential on a highly maneuverable fighter.

2. Detailed layouts of the select planforms were then made, and point-design structural weight, aerodynamic, and performance analyses were carried out.

7.1 WING PLANFORM PARAMETRIC STUDY

~~(S)~~ In Phase 1 of the study, the wing-planform selection, wing loading, aspect ratio, and leading-edge sweep angle were varied. The matrix of wing sizes and leading edge sweep angles is defined as follows:

Wing 1 (W1): AR = 3.0; W/S = 60 psf; Λ = 35°, 40°, 45°, 50°

Wing 2 (W2): AR = 3.5; W/S = 70 psf; Λ = 35°, 40°, 45°, 50°

Wing 3 (W3): AR = 4.0; W/S = 80 psf; Λ = 35°, 40°, 45°, 50°

Wing 4 (W4): AR = 4.5; W/S = 90 psf; Λ = 35°, 40°, 45°, 50°

~~(S)~~ Airplane planform comparisons are shown in Figure 7.1-1 through 7.1-4 at the four wing sweep angles for Wings 1, 2, 3, and 4 of the matrix. (The letters A, B, C, D in the figures signify wing sweeps at 35, 40, 45, and 50 degrees, respectively.) A comparison is shown in Figure 7.1-5 for the 35-degree-wing-sweep case with the four different wings delineated above and the tail sizes associated with each. Similar data are shown in Figure 7.1-6 for the 45-degree-wing-sweep case at a constant 60-psf wing loading.

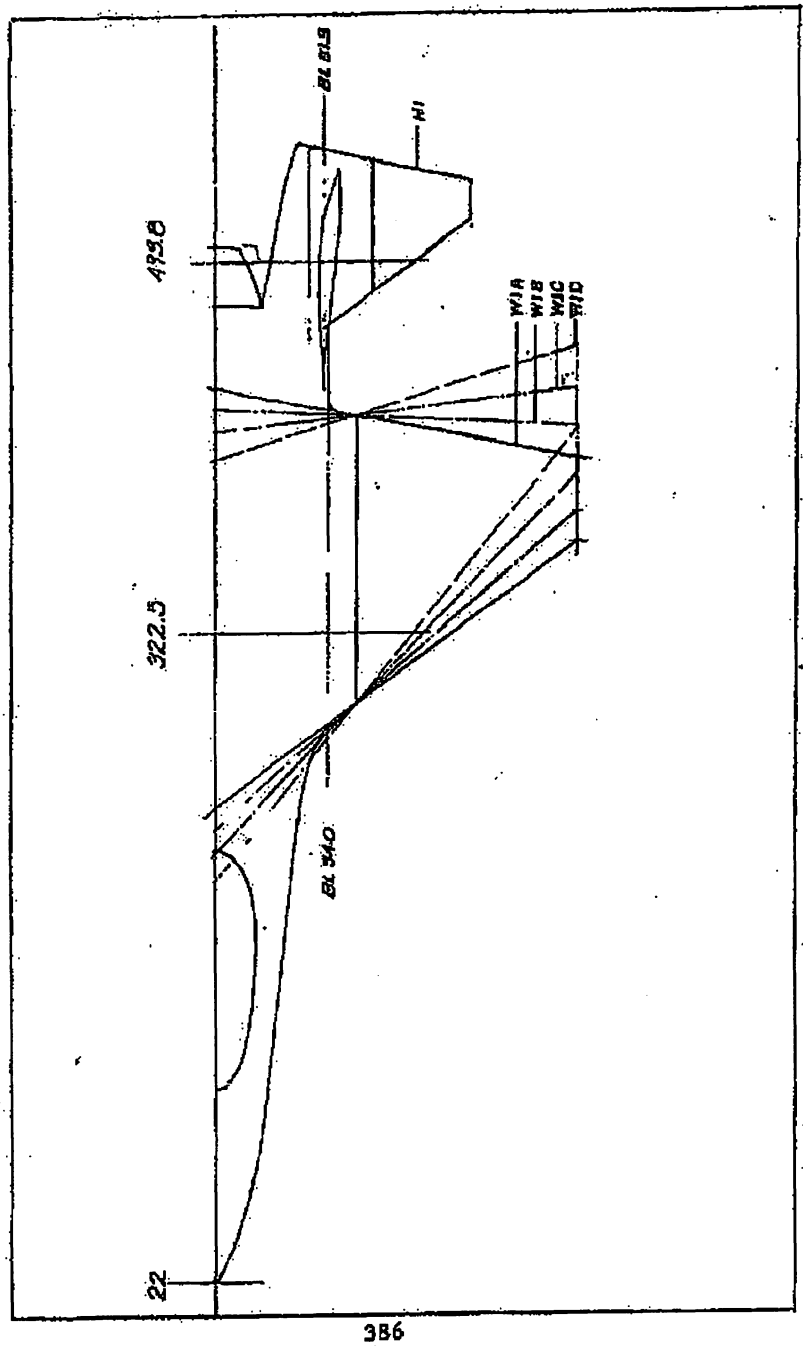

~~(c)~~ Figure 7.1-1 Supercritical Wing Family at AR= 3.00 and W/S = 60 psf (U)

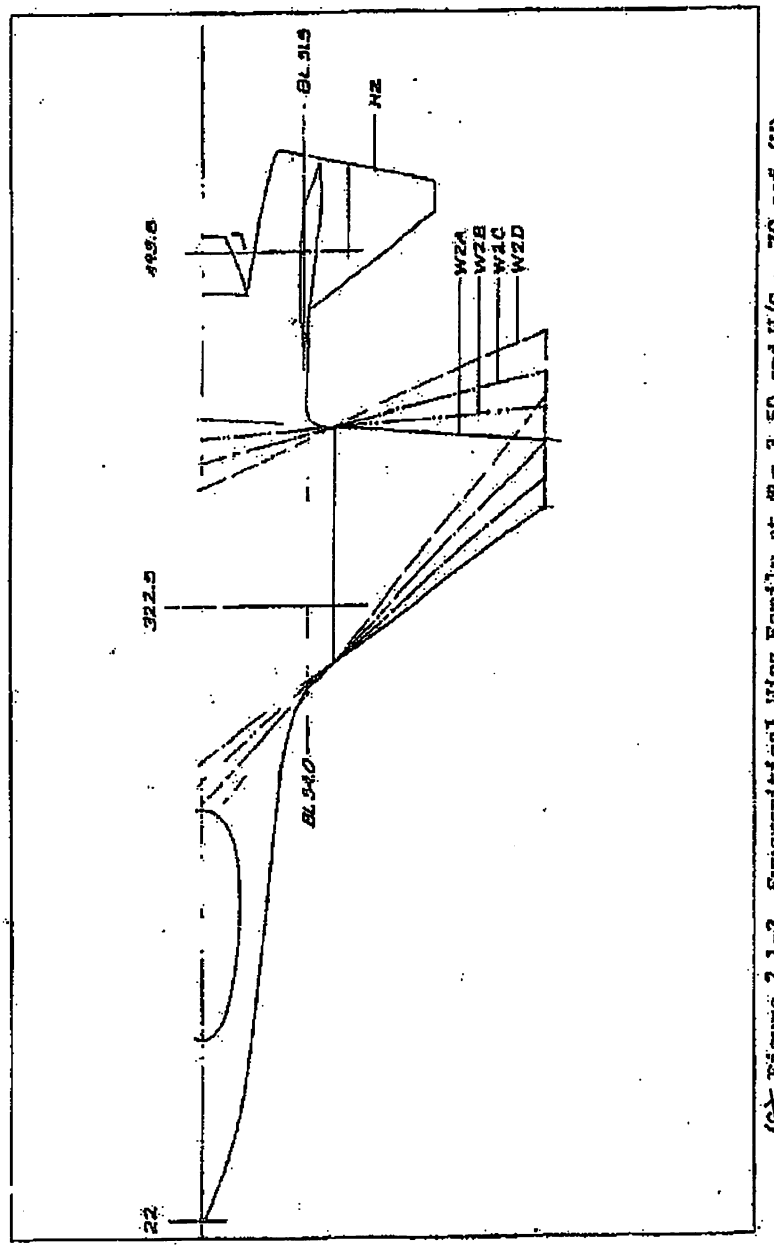

~~(C)~~ Figure 7.1-2 Supercritical Wing Family at AR = 3.50 and W/S = 70 psf (U)

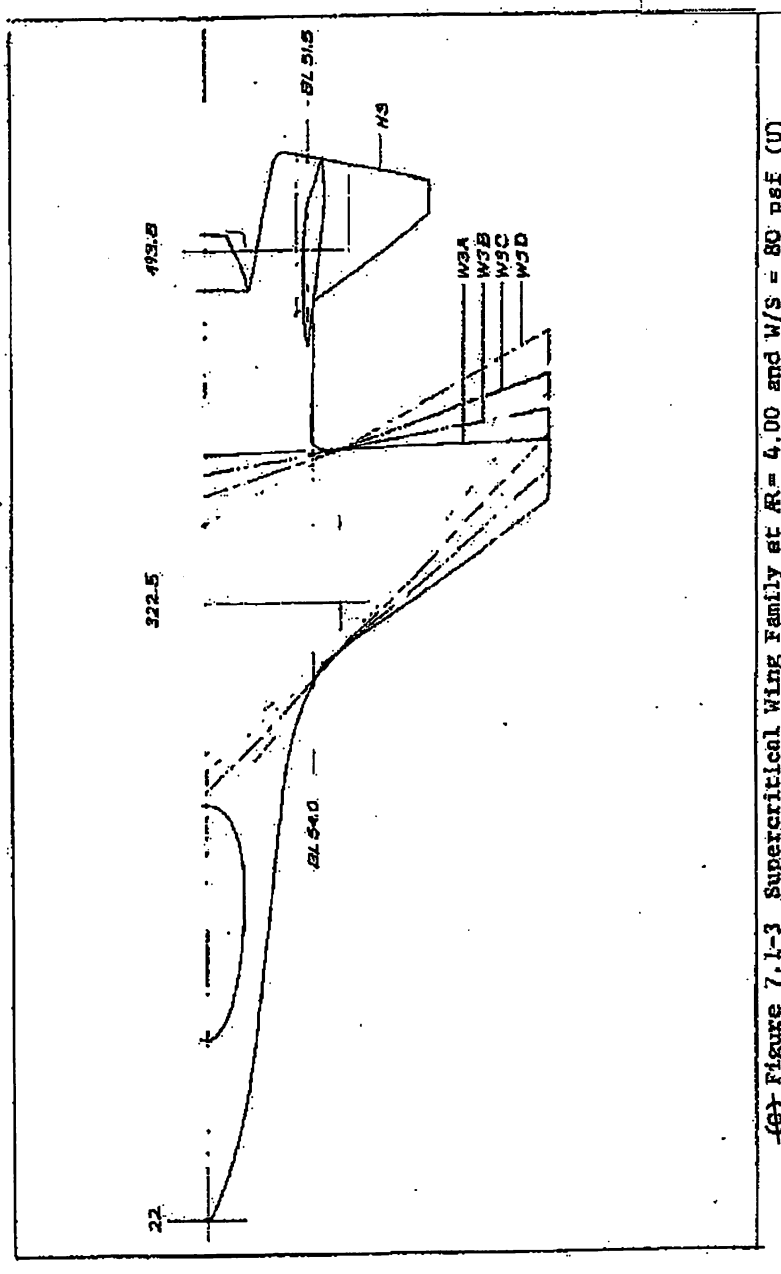

~~(U)~~ Figure 7.1-3 Supercritical Wing Family at AR = 4.00 and W/S = 80 psf (U)

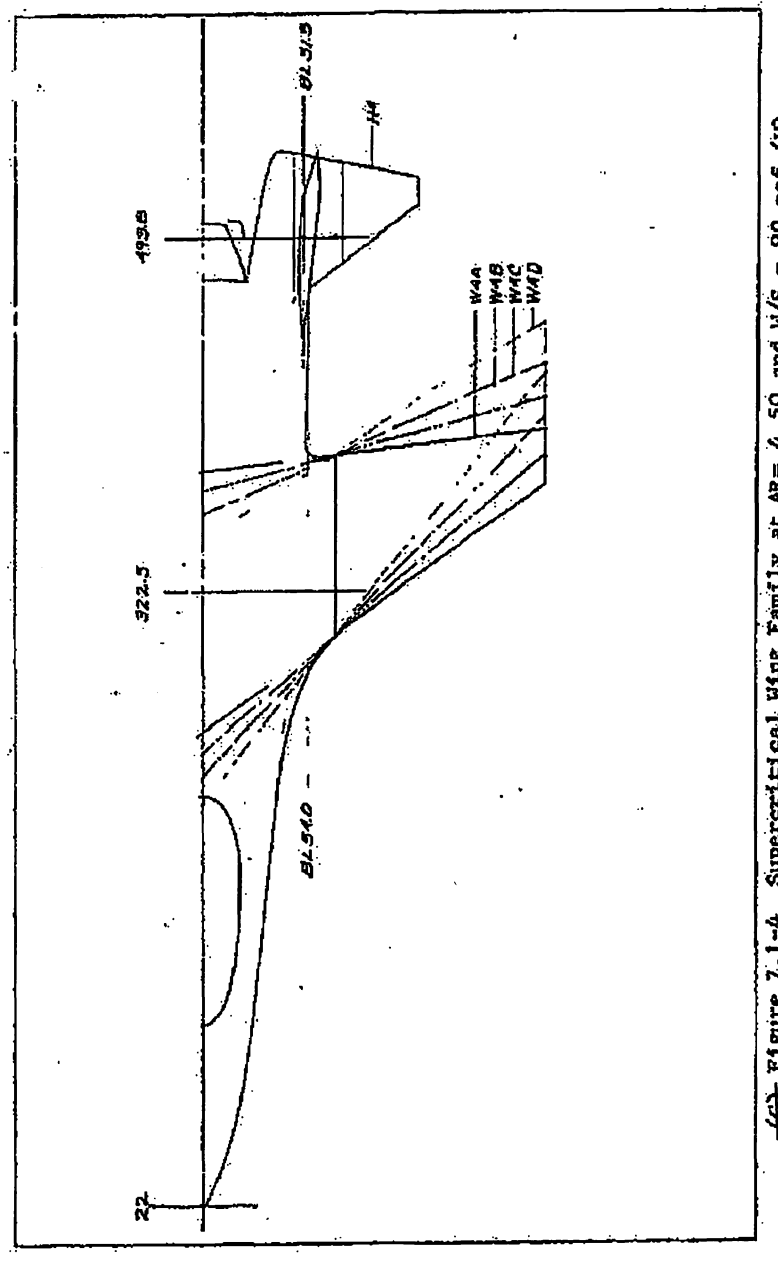

~~(C)~~ Figure 7.1-4 Supercritical Wing Family at AR= 4.50 and W/S = 90 psf (U)

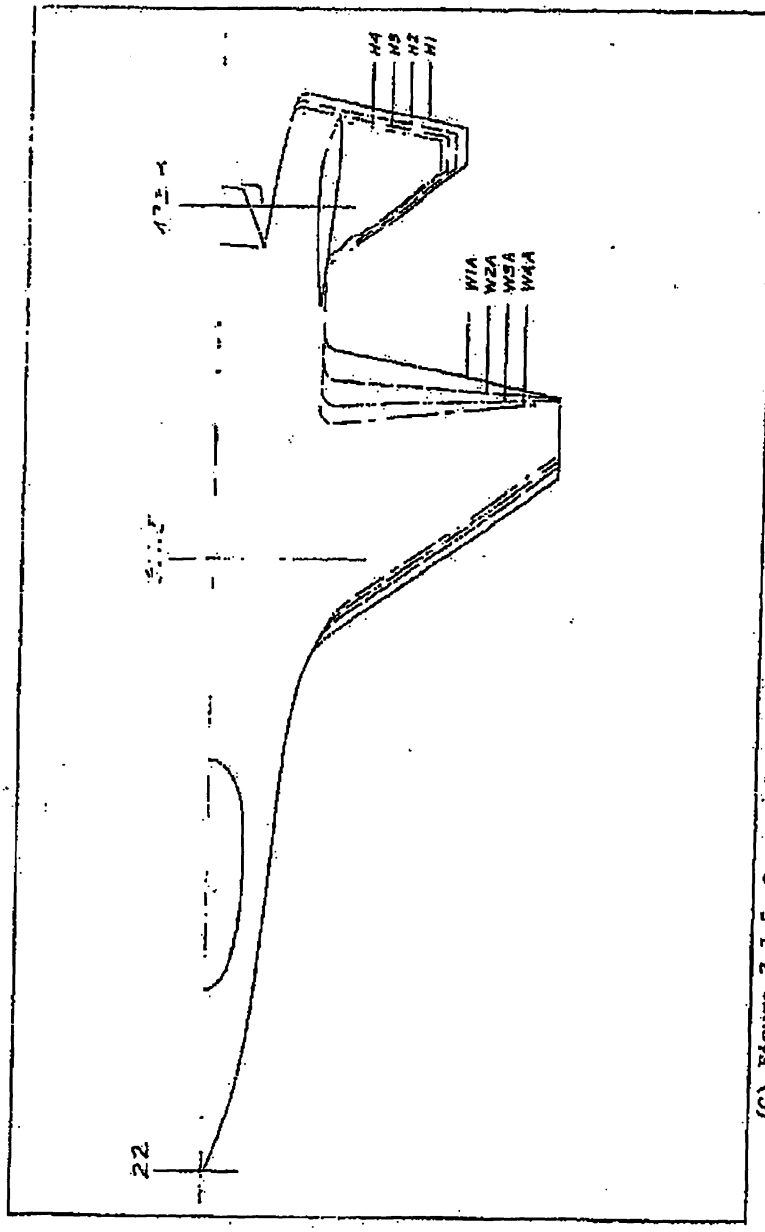

~~(C)~~ Figure 7.1-5 Supercritical Wing Family of Wing-Loading/Aspect-Ratio's at L.E. Sweep = 35° (U)

(C) Figure 7.1-6 Supercritical Wing Family of Aspect Ratios at L.E. Sweep = 45°
and Wing Loading = 60 psf (U)

~~(S)~~ In the study, taper ratio, λ, was held constant at a value of 0.2. Wings with less taper (higher taper ratios) tend to be heavier, while wings with more taper are prone to flutter and pitchup because of early tip stall.

~~(S)~~ A wing thickness ratio of 0.06 was used for all planforms considered. Experience gained in the application of supercritical airfoils to wings of several types (including F-111, F-111 TACT, B-1, FX) indicates that the potential payoff reduces as wing t/c reduces. As a result of this experience and in consultation with Dr. R. T. Whitcomb of NASA Langley, it was decided to limit the t/c of this study to 0.06 or greater.

~~(S)~~ The following list summarizes the ground rules that were established in conjunction with the matrix of variables previously described for generating the required aircraft design data:

1. Aircraft gross weight remains constant (16,800 lb).
2. The $\bar{c}/4$ of all reference wings is located at a constant fuselage station.
3. The horizontal tail moment arm is held constant (171.3 in.).
4. The wing thickness and taper ratios are held constant (t/c = 0.06, λ = 0.2).
5. The vertical tail geometry and position is held constant ($S_{H.T.}$ = 22.12 ft^2, AR = 1.3265, λ = 0.4, Λ_{LE} = 45°)
6. The "d" distance to the exposed wing root chord is held constant (54 in., measured from airplane centerline).
7. The sizing horizontal tail geometry characteristics (AR = 3.0, λ = 0.2, and Λ_{LE} = 35°) remain constant.
8. The "d" distance to the exposed horizontal tail root chord remains constant (51.5 in., measured from airplane centerline).

(S) 9. The ratio of the exposed horizontal tail area to the sizing horizontal tail area remains constant (0.866).

10. An initial sizing horizontal tail is determined by a horizontal tail volume coefficient of 0.26 and by wing geometry defined by AR = 3.0, λ = 0.2, W/S = 60 psf. This establishes a horizontal-tail-area/wing-area ratio of 0.202. As the wing geometry changes because of variations in aspect ratio and wing loading, the sizing horizontal tail area is established by keeping the area ratio of 0.202 constant.

(U) Since the primary interest is in maneuverability, the parametric comparison plots were constructed on the basis of two maneuver parameters:

1. Maximum sustained load factor at Mach .8, .9, .95, and 1.2 at 30,000 ft.

2. Energy rate for 1-g flight at Mach 0.9 at 10,000 ft.

(U) The weight and aerodynamic data used and the performance results obtained are presented in the following subsections.

7.1.1 Structures and Weights

(U) The weight analysis for the parametric study was performed with the same techniques discussed in Section 3.5. The results of this study are shown in Figures 7.1-7 and -8. It is noted that the leading-edge maneuver flap has been replaced by a fixed leading edge and that the weights reflect this change.

7.1.2 Aerodynamics

(U) The minimum drag and drag due to lift are computed by the methodology documented in Reference 1. The primary impact of the supercritical airfoil is manifested in the increase in drag divergence Mach number, which is determined from the following equation:

(S) Figure 7.1-7 Supercritical Wing Study: Effect of Wing Sweep on Dry Weight (U)

(U) Figure 7.1-8 Supercritical Wing Study: Effect of Aspect Ratio on Dry Weight (U)

(U) $$\Delta M_{DD} = (\Delta M_{DD})_{Ref} + (t/c - 0.082)$$

The $(\Delta M_{DD})_{Ref}$, shown in Figure 7.1-9 is derived from Langley Research Center wind tunnel tests of the F-111/TACT model with supercritical airfoils. The second term of the equation corrects for difference in thickness ratio between the wings considered in this study and the wings that were tested.

(U) In addition to increasing the drag divergence Mach number, the supercritical airfoil also has the advantage of obtaining high L/D's without the use of a leading-edge flap because of the blunt leading edge. All supercritical wing configurations have a fixed leading edge and therefore offer an additional weight savings.

(U) With regard to trim drag, certain simplifying assumptions are made in the design and development of a fighter. Considerable effort is directed toward minimization of trim drag, and it is reasonable to assume that levels of trim drag comparable to those for the basic biconvex airfoil are attainable for the supercritical wing. The trim drag is computed by taking the ratio of trimmed to untrimmed drag due to lift from the Configuration 401B and applying this ratio to the untrimmed drag due to lift for the supercritical configurations.

7.1.3 Performance

(U) Realistic estimates of the maneuver performance parameters must include both aerodynamics and weights. That is

$$(n_Z)_{max} = \frac{\text{lift @ max thrust}}{\text{combat weight}}$$

and

$$P_S = \frac{\text{max thrust - drag}}{\text{combat weight}} \times \text{velocity for 1-g flight}$$

where

$$\text{combat wt.} = (\text{combat wt})_{\substack{401B \\ \text{Baseline}}} + \Delta\text{combat wt.}$$

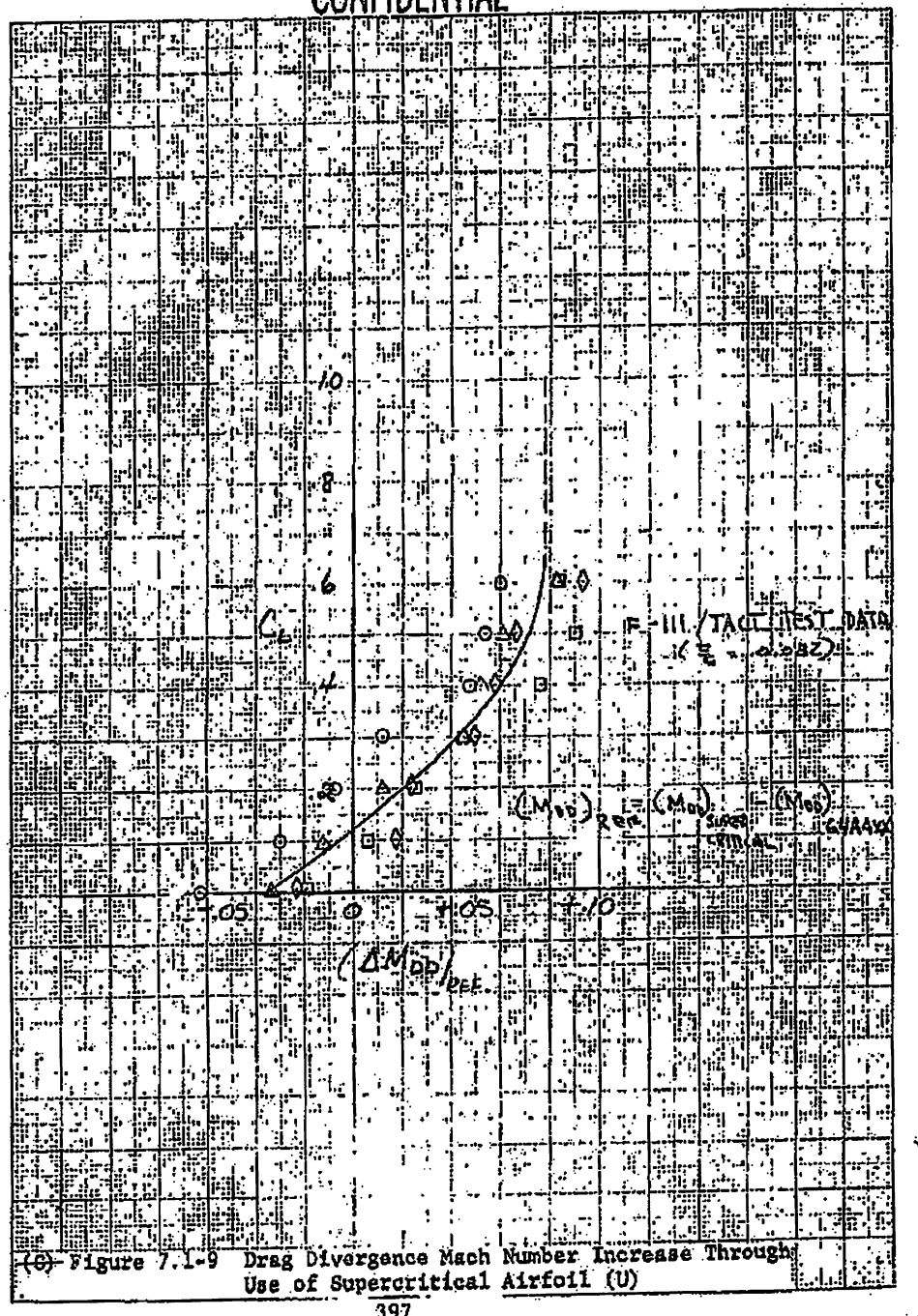

(C) Figure 7.1-9 Drag Divergence Mach Number Increase Through Use of Supercritical Airfoil (U)

Previous studies show that the change in combat weight may be approximated by the simple equation

$$\Delta \text{Combat wt} = 2.25 \times \Delta \text{structural wt.}$$

(U) The results of the parametric study are summarized in Figures 7.1-10 through 7.1-13 in the form of comparisons of the selected maneuver parameters.

(U) The effect of sweep at constant aspect ratio (3.0) is shown in Figure 7.1-10, where it is seen that increasing sweep generally improves both n_{max} and P_s up to about 45 degrees. This is a good example of the tradeoff between weight and aerodynamics. Performance data for Configuration 401B (with biconvex wing) are shown in the figure for reference. The supercritical wing provides larger load-factor values at subsonic speeds and slightly smaller values at Mach 1.2. The supercritical airfoil also has a lower energy rate (P_s) at the Mach 0.9 1-g condition at a wing leading edge sweep of 35 degrees. This is due to the higher minimum drag of the blunt supercritical wing as compared to the sharp biconvex wing. As wing leading-edge sweep is increased, the minimum drag is reduced so that the energy rate for the supercritical airfoil exceeds that for the biconvex wing at sweep angles above 40 degrees.

(U) The effects of varying wing loading at constant span, b, are shown in Figures 7.1-11 and -12. Obviously, changing wing loading with span held constant requires aspect ratio (b^2/S) to vary along with wing loading (W/S). The result is to keep induced drag (C_{D_i}) constant (for a given lift) so that the pure effect of wing size (S) can be observed, i.e., $C_{D_i} = C_L^2/\pi (b^2/S)\, e$. It is seen that increasing wing loading improves the sustained load-factor capability and degrades the 1-g energy rate. The increased turn rate (higher n_z) for the W/S = 60 psf supercritical wing configurations ($\Lambda = 35^\circ$ and 45°) at subsonic speeds, relative to the basic 401B, indicates a greater lift per unit area for the supercritical wing section. The 45-degree-sweep supercritical wing configuration of Figure 7.1-12 also shows a higher energy rate (P_s) than the basic 401B wing configuration.

(U) The $\Lambda = 45^\circ$, W/S = 60 psf (AR = 3.0) planform was selected as the best compromise for the aspect-ratio variation. This effect is summarized in Figure 7.1-13. At subsonic speeds it is seen that increasing AR improves n_z but degrades the 1-g P_s at Mach 1.2; n_z reaches an optimum at about AR = 3.5.

(U) It becomes readily apparent that no one planform is best for all conditions; therefore, the selected planforms will necessarily be a compromise. Two planforms were selected for detailed analysis.

(1) AR = 3.75 (AR = 4.0 with curved tips)

$\Lambda = 45^{\circ}$

W/S = 60 psf

(2) AR = 3.0 (AR = 3.2 with curved tips)

$\Lambda = 45^{\circ}$

W/S = 60 psf